stellarator news

Published by Fusion Energy Division, Oak Ridge National Laboratory
Building 5700 P.O. Box 2008 Oak Ridge, TN 37831-6169, USA

Editor: James A. Rome Issue 94 September 2004
E-Mail: jar@ornl.gov Phone (865) 482-5643
On the Web at *http://www.ornl.gov/sci/fed/stelnews*

Recent QPS progress

The Quasi-Poloidal Stellarator (QPS) project has achieved two significant programmatic milestones recently. In May the U.S. Department of Energy (DOE) approved Critical Decision 1 for the QPS project, which sets the configuration and cost range for the project. This follows a successful DOE conceptual design review held in June 2003.

The most complex QPS component is the set of 20 modular coils, four each of 5 different shapes, shown in Fig. 1.

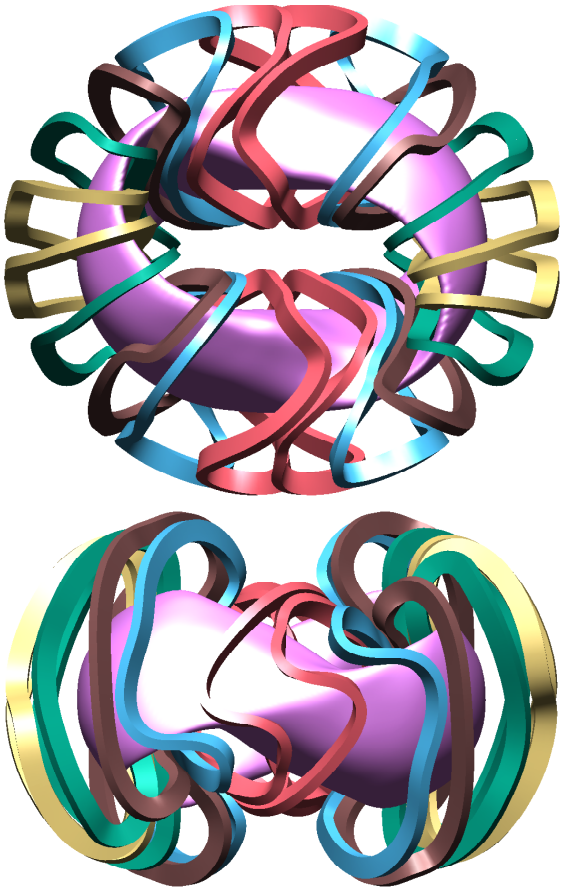

Fig. 1. The last closed QPS flux surface and the modular coil set that creates it.

In this issue . . .

These coils are arranged in pairs, in the three different types of modular coil winding forms. For each of the two field periods, the two red coils (Fig. 1) in the center of the long section are in one winding form (the one being fabricated), the blue and brown coils are in a second type of winding form, and the yellow and green are in the third type of winding form, the one illustrated in Fig. 2. The individual winding forms are bolted together to form a structural shell with large penetrations for diagnostic and heating access. Figure 2 shows how a completed shell segment, containing a yellow and green coil in Fig. 1, is fabricated. Conductors are wound directly on the machined winding forms, a vacuum-tight can is welded to the structure, the windings are vacuum/pressure impregnated with epoxy, and clamps are attached to the structure. In August, a contract was awarded for fabrication of one of the highly accurate, stainless steel cast forms on which a prototype coil will be wound. Delivery of the casting is projected for December. Fabrication of the full-scale prototype casting will demonstrate the feasibility of casting what is perceived to be the most difficult shape, that containing the red coils in Fig. 1. It will provide a basis for follow-on work that includes finish machining of the casting and a fixed price and schedule proposal for production of the ten winding forms.

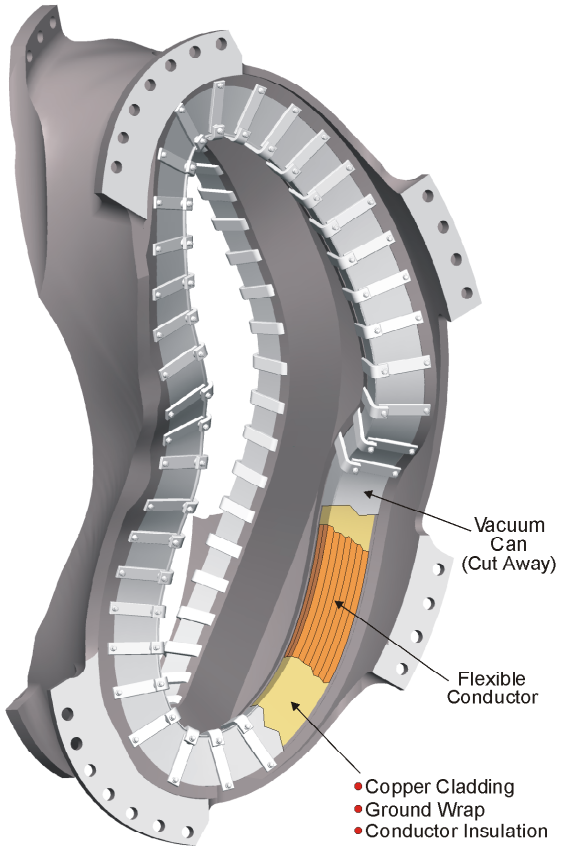

Fig. 2. Cutaway view of a fabricated QPS shell segment.

James F. Lyon
Oak Ridge National Laboratory
P.O. Box 2008, Oak Ridge, TN 37831-6169, USA
Phone: (865) 574-7179
E-mail: lyonjf@ornl.gov

Wendelstein 7-X planar coil test

Work is proceeding on the Wendelstein 7-X stellarator at IPP Griefswald. Figure 1 shows one of the superconducting planar coils for W7-X during an assembly test at IPP Greifswald at the end of August. The auxiliary set of 20 noncircular planar coils — 2 per half-period — provides the major degree of freedom in the flexibility of the stellarator magnetic configuration. For example, the planar coils can vary the edge rotational transform ($0.83 < \iota(a) < 1.20$) as well as the effective vertical magnetic field. The planar coils enclose the 50 nonplanar coils which themselves provide the standard magnetic field configuration.

Fig. 1. The picture shows a coil handling unit with one of the coils during the tests, providing training of the stuff involved. Tracking the 2.2 tons of a planar coil over the set of nonplanar coils of a preassembled half-module requires highly precise motion using all 6 degrees of freedom. During this process, the minimum distances to the nonplanar coils are about 1 cm. (Photo: B. Kemnitz)

Matthais Hirsch
Max-Planck-Institut für Plasmaphysik
Teilinstitut
D-17491 Greifswald, Germany
Phone: +49-3834-88-2536
E-mail: Matthias.Hirsch@ipp.mpg.de

Experimental evidence of coupling between sheared flow development and turbulence in the TJ-II stellarator

One of the important achievements of the fusion community has been the development of techniques to control plasma fluctuations based on the mechanism of shear stabilization. When the shear rate approaches the characteristic frequency of the turbulence, a reduction in the turbulence amplitude is predicted. $\boldsymbol{E} \times \boldsymbol{B}$ shear stabilization mechanisms play a key role in the development of edge and core transport barriers. These results emphasize the importance of clarifying the driving mechanisms of sheared flows in fusion plasmas.

A reversal in the perpendicular phase velocity of fluctuations (v_θ) has been observed in the proximity of the last closed flux surface (LCFS) in all magnetic fusion devices. Here we show that the generation of spontaneous sheared flows is coupled with an increase in the level of edge turbulence in the TJ-II stellarator [1].

Experiments were carried out in electron cyclotron resonance heated (ECRH) plasmas [$P_{\mathrm{ECRH}} = 200$ kW, $B_\mathrm{T} = 1$ T, $R = 1.5$ m, $\langle a \rangle \approx 0.22$ m, $\iota(a) \approx 1.7$]. Plasma density was systematically modified in the range $(0.3–0.8) \times 10^{19}$ m^{-3}. Radial profiles and fluctuations were simultaneously measured at the plasma edge using Langmuir probes.

Profiles of the average ion saturation current, the floating potential, $\boldsymbol{E} \times \boldsymbol{B}$ turbulent transport ($\Gamma_{\boldsymbol{E}\times\boldsymbol{B}}$), and the perpendicular phase velocity for plasmas with different line-average density are shown in Fig. 1. As plasma density increases, the edge ion saturation current and its radial gradient increase, and the floating potential becomes more negative at the plasma edge. Because the edge temperature profile (in the range of 20–30 eV) is rather flat in the TJ-II plasma periphery, the radial variation in the floating potential signals directly reflects changes in the radial electric field, which turns out to be radially inward in the plasma edge as density n increases above 0.5×10^{19} m^{-3}.

The local $\boldsymbol{E} \times \boldsymbol{B}$ turbulent transport [$\Gamma_{\boldsymbol{E}\times\boldsymbol{B}} = \langle \tilde{n}(t)\tilde{E}_\theta(t)\rangle / B$] remains radially rather constant and small in low-density regimes. Local turbulent particle flux also shows an increase near the critical density ($n \approx 0.5 \times 10^{19}$ m^{-3}) and tends to slightly decrease as sheared flow develops. During the development of the shear layer (i.e., above the critical plasma density), $\boldsymbol{E} \times \boldsymbol{B}$ increases about a factor of ten in the plasma edge ($\rho \approx 0.9–0.95$), whereas $\boldsymbol{E} \times \boldsymbol{B}$ decreases when moving radially outward.

The perpendicular phase velocity of fluctuations is radially flat for plasma density below 0.5×10^{19} m^{-3}, whereas above this critical density the poloidal phase velocity reverses and the naturally occurring velocity shear layer appears in the proximity of the LCFS.

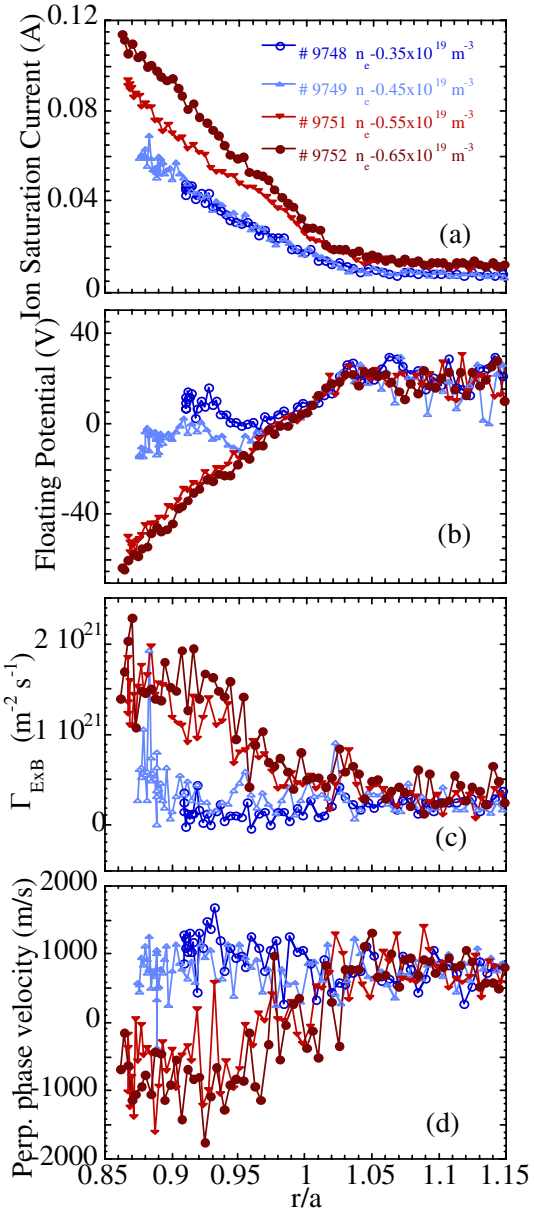

Fig. 1. Radial profiles of (a) ion saturation current, (b) floating potential, (c) $\boldsymbol{E} \times \boldsymbol{B}$ turbulent transport, and (d) the perpendicular velocity obtained for different values of the line-average density in TJ-II plasmas (shot 9748: 0.35×10^{19} m^{-3}, shot 9749: 0.4×10^{19} m^{-3}, shot 9751: 0.55×10^{19} m^{-3}, shot 9752: 0.65×10^{19} m^{-3}). Experiments were carried out in a magnetic configuration with $\iota(a) \approx 1.7$.

The magnitude of the spontaneously developing shearing rates (dv_θ/dr) has been compared with those measured during biasing-induced improved confinement regimes in TJ-II [2]. For the biasing experiments, one limiter was localized up to 2 cm inside the LCFS and biased ($\Delta V_{limiter}$ = 160–250 V, $I_{limiter} \approx$ 30–50 A) with respect to the second mobile outer limiter located in the scrape-off layer region (0.5 cm beyond the LCFS). The evolution of shear rates and fluctuation levels with plasma density are shown in Fig. 2 for spontaneous and biasing-induced sheared flows. During the transition to improved confinement regimes induced by limiter biasing, a clear reduction in the $\boldsymbol{E} \times \boldsymbol{B}$ turbulent flux has been observed. It is remarkable that the shear rates observed during improved confinement regimes are comparable to those observed to be associated with the naturally occurring shear layer. This result shows that spontaneous sheared flows and fluctuations are near marginal stability.

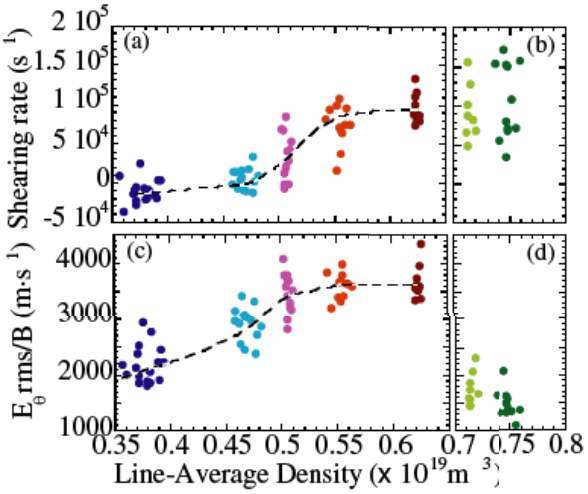

Fig. 2. Comparison of spontaneous and biasing-induced sheared flows and fluctuations at the plasma edge (($r/a \approx$ 0.9): (a) spontaneous and (b) biasing-induced shear rates; (c) spontaneous and (d) biasing-induced radial velocity fluctuations. Different colors represent data from different shots. Dotted lines are provided as visual guides.

The electron density profile shows a broadening above the critical density while the temperature profile remains largely unchanged, reflecting the strong impact of plasma density in the TJ-II global confinement scaling.

In conclusion, the development of the naturally occurring velocity-shear layer requires a minimum plasma density in the TJ-II stellarator. Near the critical density, where the sheared flow is developed, the level of the edge turbulent transport and the turbulent kinetic energy significantly increase. The resulting sheared flow is close to that required to reduce turbulent transport (as measured during biasing-induced improved confinement regimes), showing that spontaneous sheared flows and fluctuations are near marginal stability. These results have a direct impact in our understanding of the physics mechanisms underlying the generation of critical sheared flows, pointing out the important role of turbulence-driven flows.

M. A. Pedrosa,* C. Hidalgo, E. Calderón, T. Estrada, A. Fernández, J. Herranz, I. Pastor, and the TJ-II team
Laboratorio Nacional de Fusion
Asociación EURATOM-CIEMAT
Avda Complutense 22, 28040 Madrid, Spain

*E-mail: angeles.pedrosa@ciemat.es

References

[1] M. A. Pedrosa et al., "Direct experimental evidence of coupling between sheared flows development and increasing turbulence in the TJ-II satellarator."paper O4-04 presented at the 31st European Physical Society Conference on Plasma Physics, London, 2004.

[2] C. Hidalgo et al., Plasma Phys. Control. Fusion **46** (2004) 287.

Accuracy of the magnet configuration of Wendelstein 7-X

1. Introduction

Wendelstein 7-X (W7-X) is in an advanced construction phase, and assembly will start in autumn 2004. The magnet system of W7-X is composed of 50 nonplanar and 20 planar superconducting coils that are arranged in five equal modules. The coils are bolted to a central coil support structure and mutually supported by intercoil supports [1]. To achieve the goals of optimized stellarator confinement for which W7-X has been designed, the coils need to be constructed and assembled with high precision. Small statistical deviations from the ideal coil shape or nonsymmetric alignment could result in field perturbations with a periodicity different from the five-fold periodicity of the device. The errors would cause enhanced particle losses, additional magnetic islands, ergodization of the existing islands, and a possible asymmetric load on the divertor targets. In particular, the stellarator symmetry of the machine must be achieved despite the modular character of the coil system. Therefore the accuracy of the magnet configuration is an important issue for coil construction and system assembly during the W7-X project.

Fig. 1. Dimensional control of a nonplanar winding package using a Faro arm. The reference pins are positioned on circular plates mounted on the dark-colored part of the coil, (i.e., on the left-hand side of the measuring technician).

2. Outline of the design and assembly

Winding of the nonplanar (planar) coils requires forming of 108 (36) turns of a cable-in-conduit superconductor into precisely machined winding forms. Conformance with the required shape is checked by careful control of some 800 positions along the four sides of the surface of the winding package (Fig. 1). A best fit of the measurement data defines the coordinates of eight precise reference pins (see Fig. 1) mounted on the surface of the winding package. These pins carry the basic geometry information of the winding and are used as reference during all further manufacturing processes, as well as during assembly. The winding packages are integrated and embedded in steel casings using glass fiber-reinforced epoxy pads, glass balls, quartz sand, and epoxy resin (Fig. 2). The interfaces of the coil casing as well as the threads and holes, which are used for fixation and adjustment, are machined to an accuracy of a few tenths of a millimeter. After the winding packages are embedded in the steel casings, and after final machining of the interface areas, the positions of the reference pins are checked for any deformations. Finally, the contours of the surface of the casing are checked against the pin positions as well as against the computer-aided design (CAD) model.

Fig. 2. Embedding a winding package into the steel casing of a nonplanar coil.

Assembly of the magnet structure starts by stringing the coils across the plasma vessel (Fig. 3) and adjusting them into their nominal position. Half-modules of the magnet system are formed by joining five nonplanar and two planar coils to a sector of the central coil support unit. Two half-modules are bolted to form magnet modules. After completion of the five magnet modules along with the outer vessel, the ports, and the thermal insulation, they will all be positioned on the machine base and joined to form a torus.

3. Accuracy requirements

As a general rule, nonsymmetric disturbances of the magnetic field $\Delta B/B_0$, where B_0 is the toroidal field on the axis, must be small, whereas symmetric disturbances (e.g., systematic deviations of the shape and position of a coil) are less critical. As a design criterion, Fourier components ΔB_{mn} of the W7-X field must be smaller than $2 \times 10^{-4}\, B_0$, where m denotes the toroidal and n the poloidal index of the Fourier component [2]. Most dangerous are the low-order Fourier harmonics B_{11} and B_{22}, which are resonant

to the major rotational transform $\iota = 1$ and which break the stellarator symmetry of W7-X. As a consequence, the manufacturing tolerance of the first nonplanar winding package of each type is, e.g., 5 mm, whereas the repetition tolerance of subsequent coils is ±3 mm for the inner walls, ±3 mm for the side walls, and ±5 mm along the outside of the winding packages.

Fig. 3. Stringing of a nonplanar coil across the plasma vessel using the coil stringing unit

4. Results of the metrology surveys

By the end of June 2004, 32 nonplanar and 17 planar winding packages had been wound and impregnated and five nonplanar coils and three planar coils had been completed. The shapes of the nonplanar winding packages are surveyed by laser tracking and a Faro arm, whereas the planar coils are surveyed by photogrammetry. These techniques ensure a measurement accuracy of better than 0.3 mm. From the measured coordinates of the surface of the winding package, the geometry of the central current filament of the coil is deduced. The geometry of the current filament is compared with its nominal geometry as well as with results of the surveys of already manufactured winding packages of the same type. As an example, Fig. 4 shows the measured radial deviations of the central current filament of six nonplanar winding packages of type 1 from the design geometry. The data show an average systematic deviation from the CAD model of <2.9 mm and an average statistical deviation from the average filament geometry of <1.1 mm.

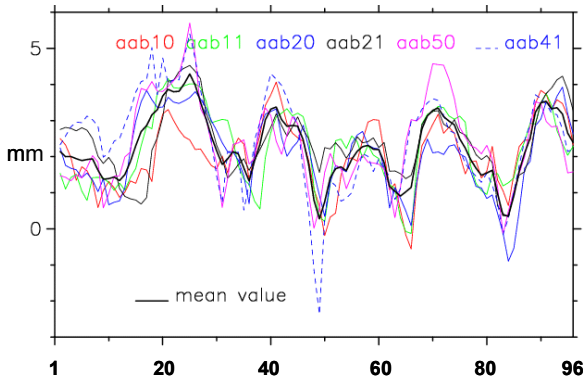

Fig. 4. Radial deviation of the central filaments of six coils along the circumference. The reproducibility is rather high; systematic deviations result from the process of bending the superconductor into the highly precise form.

5. Analysis of the survey

A numerical code was established to assess the impact of deviations during coil manufacture on the magnetic configuration of W7-X [3]. Evaluation of the central current filaments of a total of 27 manufactured nonplanar winding packages shows an average systematic error of <3 mm and statistical deviations below 1 mm. Assuming that all nonplanar winding packages follow the average shape of those already manufactured, the dominant Fourier components $\Delta B_{11}/B_0$ and $\Delta B_{22}/B_0$ would account for 0.4×10^{-4} and 0.5×10^{-4} (respectively) of the total field errors. (Note that ΔB_{mn} must be smaller than $2 \times 10^{-4}\ B_0$.) The code also allows simulation of misalignment during assembly and offers suggestions for corrective measures. The errors during assembly result from misalignment of the coils, distortions during welding of the lateral supports, and small errors during the adjustment of the half-modules and modules. Numerical analyses (Fig. 5) have shown that rotational misalignment of components has a greater impact on the field errors than radial or lateral shifts of the components. From assembly trials it is concluded that each reference point on coils, half-modules and modules can be positioned to be accurate to within a sphere with a radius of 1.5 mm. Statistical extrapolation of the inaccuracies occurring during all assembly steps while considering the accuracy of measurement result in an average error of the position of each coil of 3.5 mm. A simulation of these errors during assembly shows Fourier components $\Delta B_{11}/B_0$ and $\Delta B_{22}/B_0$ equal to 2.8×10^{-4} and 1.4×10^{-4}. Thus, it is evident that assembly errors contribute significantly more to the final field error than manufacturing errors of individual coils and might even be critical in achieving the specified limit.

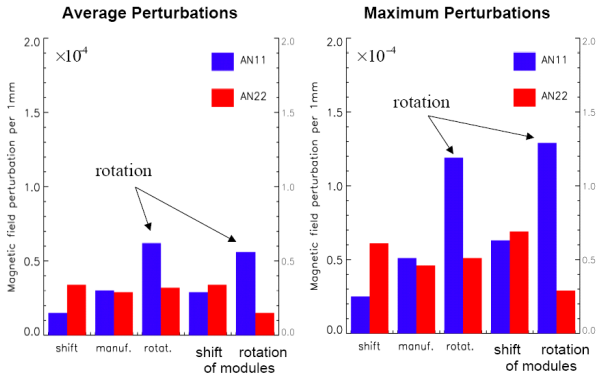

Fig. 5. Relative magnetic field perturbation resulting from an average deviation of 1 mm caused by different types of coil errors. Shown are the two most critical Fourier components, $\Delta B_{11}/B_0$ and $\Delta B_{22}/B_0$. The magnetic field is most sensitive to rotation of coils or whole modules.

6. Measures for correction

Final assembly of the torus allows adjustment of the position of each corner of the modules within a 5-mm-radius-sphere by applying shims between the module sectors of the coil support structure. This correction measure could reduce the B_{11} and B_{22} components by ~ $2 \times 10^{-4}\ B_0$. In addition, during W7-X operation ten control coils behind the divertor can be used to compensate B_{11} field components by up to $1.6 \times 10^{-4}\ B_0$. Additional compensation of field errors could be achieved by extra coils outside the outer vessel [2].

M. Wanner,[1] T. Andreeva,[1] T. Bräuer,[1] J. Kißlinger[2]
[1] Max-Planck-Institut für Plasmaphysik, EURATOM Association, Teilinstitut Greifswald, Wendelsteinstraße 1
D-17491 Greifswald, Germany
[2] Max-Planck-Institut für Plasmaphysik, EURATOM Association, Boltzmannstraße 2
D-85748 Garching, Germany
E-mail: manfred.wanner@ipp.mpg.de

References

[1] M. Wanner et al., Nucl. Fusion **43** (2003) 416.

[2] J. Kisslinger, "Possibilities for the correction and compensation of magnetic field errors in Wendelstein 7-X," Proc. 14th Int. Stellarator Workshop, Greifswald (2003).

[3] T. Andreeva et al., submitted to Fusion Sci. Technol. **46** (2004) 388.

Extended abstracts

Radiation belts in the Wendelstein-7AS stellarator

To appear in the *Journal of Nuclear Materials* (Proceedings of the 16th Conference on Plasma-Surface Interactions)

At the edge of the Wendelstein-7AS stellarator at high plasma density, we find two types of radiation belts. The first one is found in the inboard scrape-off layer (SOL) when the divertor plasma is detached. It is observed in the CIII emission at 465 nm but not in H_α (see Fig. 1). The phenomenon seems to be specific to a stellarator. Modeling results obtained by the EMC3-Eirene code explain this experimental result as follows: At low divertor temperatures, the carbon radiation moves away from the target plates (detachment process). It cannot be stabilized within the divertor plasma but only in the inboard SOL in the region of the islands. The temperature in the divertor is still high enough to excite and ionize the hydrogen atoms. Thus, the hydrogen emission dominates in the divertor but the carbon emission (CIII) is dominant in the inboard SOL. The modeling shows lower temperatures in the inboard SOL than in the outboard SOL. Consequently, the region at the divertor target plates that is connected to the inboard side detaches at first. The region connected to the outboard side of the SOL stays attached (i.e., a partial stable detachment). This kind of asymmetry is similar to the tokamak where a temperature asymmetry of the inner and outer divertor plasma has been found.

At higher density we observe a radiation belt not only in CIII but also in the light of H_α. Ray-tracing calculations suggest that this belt resides on closed flux surfaces. Thus, it resembles the MARFE phenomenon well known from tokamaks. The H_α emission originates from the center of the MARFE, which is cold and dense due to the effect of radiative condensation. It can even be recombining. The current-free stellarator plasma does not collapse as a whole, but the penetration of the radiation belt into the confinement region results in a confinement degradation and an unstable edge plasma as evidenced by large H_α oscillations. Thus, we consider discharges with a MARFE to be at the operational limit (density limit at about 4×10^{20} m^{-3} for the standard magnetic configuration).

U. Wenzel,* H. Thomsen, Y. Feng, P. Grigull, K. McCormick
Max-Planck-Institut für Plasmaphysik, EURATOM Association
D-17493 Greifswald, Germany
*E-mail: ugw@ipp.mpg.de

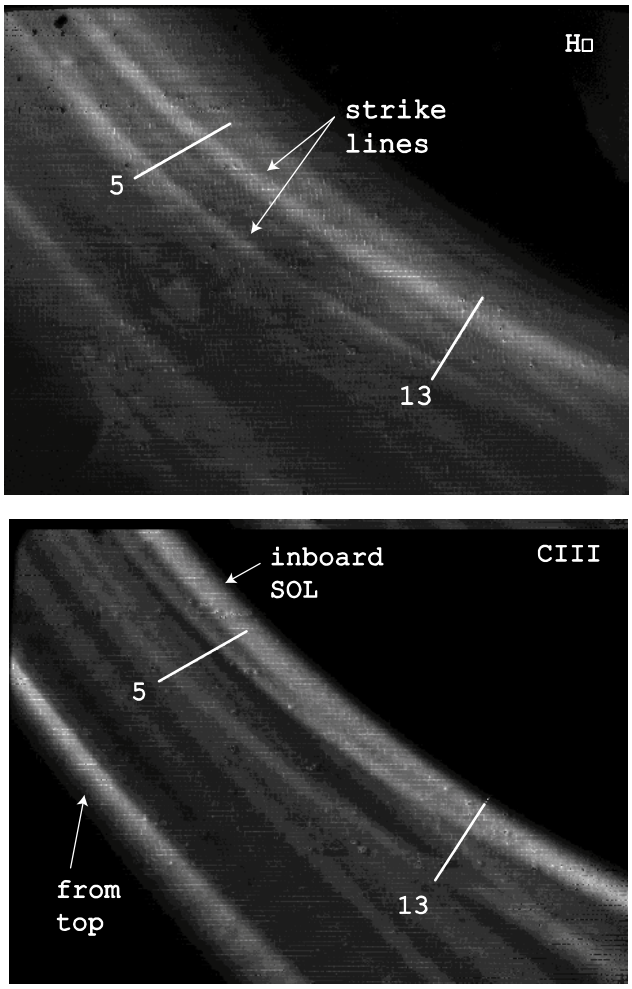

Fig. 1. View of the detached plasma in the lower divertor: H_α (top) and CIII (bottom. Data is from shot 56244 at t = 0.45 s. Divertor target tiles 5 and 13 are indicated by white lines. The H_α picture shows two strike lines from the divertor. Contrary to this, the CIII emission is dominated by a radiation belt from the inboard SOL; the carbon emission from the divertor strike lines is much weaker. The intense straight stripe in the left lower corner is an extension of a radiation zone from the upper divertor.

Meetings

A summary report on the IAEA Technical Meeting on Innovative Concepts and Theory of Stellarators held in Greifswald, 29 September–1 October 2003, has now been published in *Nuclear Fusion* (Vol. 44, Issue 5, pp. 686–688).

Additionally, talks given at the meeting can be obtained in electronic form from the Web at

http://www.ipp.mpg.de/de/for/bereiche/stellarator/TCM2003/tcm.html

The papers presented at the 31st EPS Conference on Plasma Physics, 28 June–2 July 2004, are also available on the Web at

http://130.246.71.128/